

# Preparation and Properties of Silanized Vapor-Grown Carbon Nanofibers/Epoxy Shape Memory Nanocomposites

Juan Ding, Yaofeng Zhu, Yaqin Fu

Key Laboratory of Advanced Textile Materials and Manufacturing Technology Ministry of Education, Zhejiang Sci-Tech University, Hangzhou, Zhejiang 310018, China

**Silanized vapor-grown carbon nanofiber/epoxy (silanized-VGCNF/EP) shape memory polymer (SMP) nanocomposites are successfully fabricated by using a composite molding technology. The surface functionalization of VGCNF is performed using an acid treatment followed by a reaction with silane. The oxidation as well as silanization of VGCNF and silanized-VGCNF/EP nanocomposites are systematically and explicitly characterized using various analytical methods. The influence of the silane-functionalized VGCNF on the properties of VGCNF/EP nanocomposites is investigated using field emission scanning electronic microscopy (FE-SEM) and a dynamic mechanical analysis (DMA). The shape memory properties of the silanized-VGCNF/EP nanocomposites are evaluated by a fold-deploy shape memory test. The results reveal that the silanized-VGCNF is preferably dispersed in the epoxy resin matrix. Furthermore, the glass transition temperature of silanized-VGCNF/EP nanocomposites is enhanced, and the shape memory properties of the silanized-VGCNF/EP nanocomposites are significantly improved. POLYM. COMPOS., 35:412–417, 2014. © 2013 Society of Plastics Engineers**

## INTRODUCTION

When a material is said to have the shape memory property, it can be inferred that this material can be deformed and fixed into a temporary shape and can recover its original permanent shape in the presence of external stimuli such as heat, light, and an appropriate pH value [1–3]. Shape memory polymers (SMPs) are typical shape memory materials, which are possible candidates for a wide range of applications because of their excellent processability, lightweight, and significant flexibility from the perspective of material design [4–6].

Epoxy resins merit a special mention among the diverse shape memory polymers because they are unique thermoset

shape memory polymer systems with excellent thermo-physical and mechanical properties along with exhibiting ease of processing into engineering components [7, 8].

However, the mechanical properties of epoxy deteriorate after several cycles of a process. Therefore, the improvement of the thermal and mechanical properties of epoxy and its composites has received considerable research attention [9, 10]. Furthermore, VGCNFs have attracted a considerable amount of attention as nanofillers [11–13]. For example, the introduction of VGCNFs as a structural element in polymer matrix can significantly improve the mechanical properties with a relatively low filler content; and as a conducting filler, VGCNFs can modify the transportation properties of polymer-based composites. However, if these materials are to be utilized as effective reinforcements in polymer composites, proper dispersion and good interfacial bonding between the VGCNFs and polymer matrix have to be guaranteed as VGCNFs are an inherently inert material and easy to agglomerate and entangle due to their size and high aspect ratio [14–16]. The surface modification of VGCNFs by a chemical reaction is an effective way to improve their interphase interaction with polymer matrices [17–19].

In this study, VGCNFs are functionalized by chemically modifying with highly concentrated acids and silane-coupling agents. Thus, VGCNFs are expected to be multifunctional as reinforcing fillers, and the interfacial interaction of silanized-VGCNF composites can be improved. In fact, there are only a few reports on the effects of silane-functionalized VGCNFs on the shape memory properties of VGCNF/EP nanocomposites. However, the morphological and mechanical properties of these VGCNFs and the effect of chemical functionalization on the shape memory behavior are systematically investigated in this study.

## EXPERIMENTAL

### Materials

As-received VGCNFs used in this study were obtained from Showa Denko K. K., Japan. The VGCNFs synthesized

Correspondence to: Yaqin Fu; e-mail: fyq01@zstu.edu.cn

DOI 10.1002/pc.22675

Published online in Wiley Online Library (wileyonlinelibrary.com).

© 2013 Society of Plastics Engineers

by chemical vapor deposition (CVD) had a diameter of 80 nm. 3-Triethoxysilylpropylamine (APTES) with a purity of 98 wt% (Aladdin, Shanghai, China) was used as the silane functionalization agent. Hydrogen peroxide (30 wt%), nitric acid (65 wt%), and ethanol (99 wt%) were all of analytical grade and used without further purification. Epoxy resin E-51 (WSR 618) and the curing agent were procured from Jinhong Resin Factory, China.

#### Modification of VGCNFs

**Oxidation of VGCNFs.** The impurities on the surface of VGCNFs were removed by using 30 wt%  $H_2O_2$  at 80°C for 6 h. Subsequently, the reaction product was filtered and washed with distilled water. One gram of VGCNFs was immersed in concentrated nitric acid and heated to 100°C for 6 h; the solution was constantly stirred. Acid-functionalized VGCNFs were then rinsed with deionized water until the pH of the system became neutral; these VGCNFs were then dried in an oven at 110°C.

**Silanization of VGCNFs.** A total of 0.5 g of oxidized VGCNFs was dispersed in 200 mL of ethanol through ultrasonication. Subsequently, 6 mL of ethanol/APTES mixed solvent with a volume ratio of 2:1 was added to the prepared VGCNF suspension in a beaker, and the mixture solution was reacted for silanization at room temperature for 14 h under constant stirring. After the reaction was completed, the resulting product was filtered and washed with distilled water. The silanized-VGCNFs were dried in a vacuum oven at 80°C for 12 h.

**Preparation of Epoxy Polymer.** Epoxy resin E-51 was melted at 60°C for 15 min. Then, VGCNFs were dispersed in the epoxy in a beaker, which was placed in a water bath for 30 min, the solution was constantly stirred. Subsequently, a hardener was mixed with the blend of VGCNF-epoxy resin and degassed for 30 min. The mixture was poured into a polypropylene mold, cured at 80°C for 4 h and post-cured at 100°C for 1 h to produce the silanized-VGCNF/EP.

#### Characterization of VGCNFs

Fourier transform infrared spectroscopy (FT-IR) was performed using a Nicolet 5700 FTIR spectrometer (Thermo Electron) with KBr pellets. The crystal structure of the modified VGCNFs was analyzed using an X-ray diffractometer (Rigaku Co, Japan) with  $Cu K\alpha$  radiation. XRD patterns were recorded from 5° to 80° (2 $\theta$ ) at a scanning speed of 4°/min. The morphology and the microstructure of VGCNFs were characterized using a transmission electron microscopy (TEM) system (JEM 2100F JEOL, Japan).

A field emission scanning electron microscope (FE-SEM, Ultra 55, Zeiss, Germany) was used for examining the

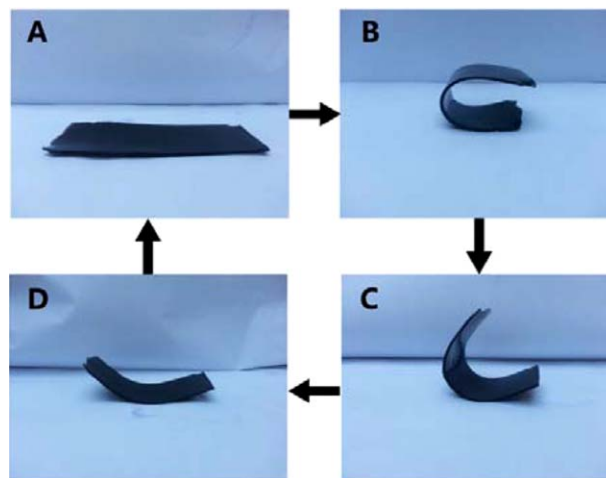


FIG. 1. Process for the shape recovery of specimens. [Color figure can be viewed in the online issue, which is available at [wileyonlinelibrary.com](http://wileyonlinelibrary.com).]

dispersion states of VGCNFs in the matrix and the fracture morphologies of the VGCNF/epoxy nanocomposites. The thermo-mechanical properties of the specimens were determined using a DMA Q800 (TA Instrument) at a frequency of 1 Hz and heated from room temperature to 120°C.

Figure 1 shows the three steps of the fold-deploy shape memory test [20]. In the first step, the samples were heated to above their  $T_g$  and then bend into a “U” shape. The maximum bending angle was recorded as  $\theta_{max}$ . Then, the U-shaped sample was cooled to room temperature under a constant external force. A marginal recovery occurred, and the bending angle became  $\theta_{fixed}$ . Finally, the packaged structure was reheated to recover its original shape. We recorded the bending angle at each temperature.

$$\text{Shape recovery ratio} : R_r = \frac{\theta_{max} - \theta_i}{\theta_{max}} \times 100\%$$

## RESULTS AND DISCUSSION

### FTIR Analysis

A schematic representation of the process of the formation of silanized-VGCNFs is given in Fig. 2. The VGCNFs are oxidized in concentrated acid. The oxygenic groups with the ethoxy groups of silane are chemically grafted on the surface of the VGCNFs.

A FT-IR analysis was performed on the unmodified, oxidized, and silane-treated VGCNFs to confirm their functionalization, as shown in Fig. 3. Figure 3a shows the FT-IR spectra of the raw VGCNF. The small peak at 3452  $cm^{-1}$  is attributed to the presence of hydroxyl groups (–OH) on the surface of the VGCNFs, which may be due to the ambient atmospheric moisture bound to the VGCNFs. Figure 3b shows the FT-IR spectra of the oxidized VGCNFs. The increase in the relative intensities of the bands at 3452  $cm^{-1}$  indicates that there are more –OH groups on the surface of the VGCNFs after the oxidation

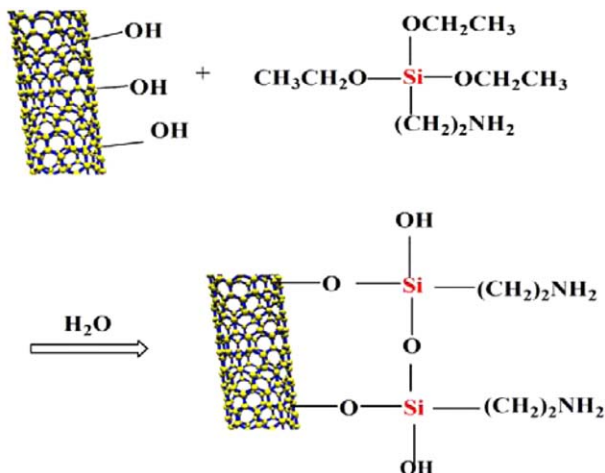


FIG. 2. Schematic representation of the reactions occurring between the reduced VGCNFs and silane. [Color figure can be viewed in the online issue, which is available at [wileyonlinelibrary.com](http://wileyonlinelibrary.com).]

[21]. A new peak that appears at  $1387\text{ cm}^{-1}$  indicates the bending vibration of the  $-\text{OH}$  group. The bands at  $1310\text{ cm}^{-1}$  correspond to the propyl chain added to the  $\text{Si}-\text{OH}$  groups, as shown in Fig. 3c. The characteristic absorption peaks at  $1123$  and  $1020\text{ cm}^{-1}$  are related to  $\text{Si}-\text{O}-\text{Si}$  and  $\text{Si}-\text{O}-\text{C}$  stretching and further support the chemical interactions between silane and VGCNFs [18, 22].

#### XRD Analysis

X-ray diffraction patterns are characterized to compare the structures of the raw VGCNFs, oxidized VGCNFs,

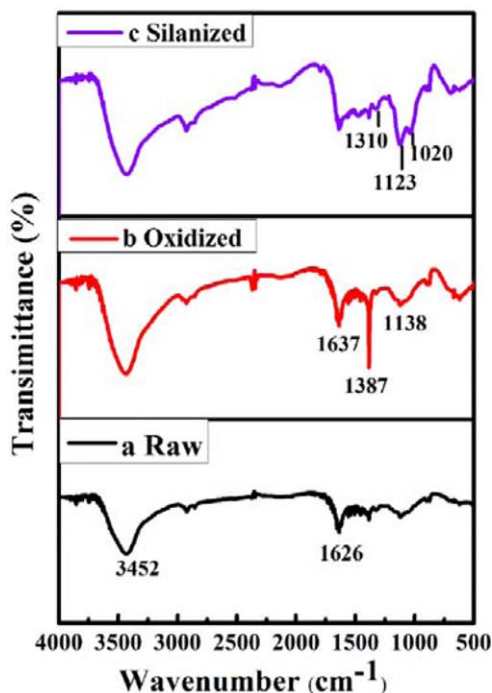


FIG. 3. FTIR spectrum of VGCNF (a: raw, b: oxidized, and c: silanized). [Color figure can be viewed in the online issue, which is available at [wileyonlinelibrary.com](http://wileyonlinelibrary.com).]

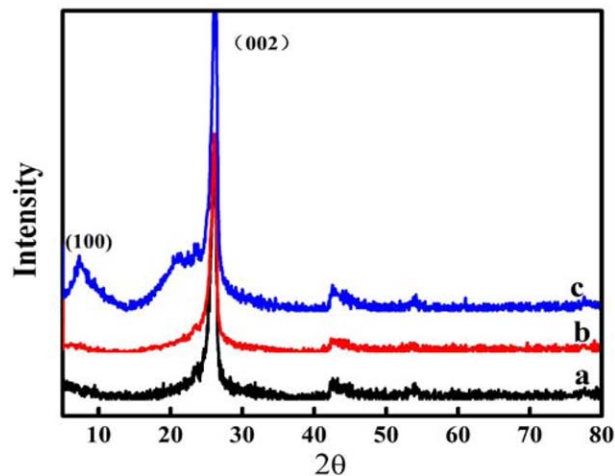


FIG. 4. XRD patterns of (a) raw VGCNFs, (b) oxidized VGCNFs, and (c) silanized VGCNFs. [Color figure can be viewed in the online issue, which is available at [wileyonlinelibrary.com](http://wileyonlinelibrary.com).]

and silanized VGCNFs, as shown in Fig. 4. The diffraction peak centered at  $26.381^\circ$  can be assigned to the graphite-structured carbons (002) of raw VGCNFs shown in Fig. 4a. Figure 4b shows oxidized VGCNFs treated by  $\text{H}_2\text{O}_2$  and  $\text{HNO}_3$ . The two sharp peaks at  $7.46^\circ$  and  $21.3^\circ$  are the characteristic peaks of silanized VGCNFs, as shown in Fig. 4c. The feature peak (002) of raw VGCNFs does not disappear after the silane treatment, indicating that silanization does not destroy the crystal structure of VGCNFs [23].

#### Surface Morphology of VGCNFs

Typical TEM images of the VGCNFs are presented in Fig. 5. Raw VGCNFs show distinct edges of the cup-stacked structure, while silanized VGCNFs show a clear coating, with a distinct interface between the VGCNFs and the silane coating, in contrast to the images shown in Fig. 5a and b [24]. The silanized VGCNFs are further characterized by HRTEM, as shown in Fig. 5c. Obviously, the VGCNFs are coated with a uniform layer. It appears that the average thickness of the coating is approximately 1–2 nm.

#### Surface Morphology of VGCNFs/Epoxy Nanocomposites

The FE-SEM images of the fracture surfaces of the composites are shown in Fig. 6. The untreated VGCNFs are mainly present in the form of agglomerates, whereas the silanized VGCNFs are well harmonized with the epoxy matrix. The unmodified composites, as shown in Fig. 6a, have a clean surface with the VGCNF-reinforced epoxy resin, indicating a poor interfacial interaction between the VGCNFs and the epoxy resin. In contrast, silanized composites (Fig. 6b) have an uneven surface [22]. It appears that well-dispersed silanized VGCNFs consume more energy in the process of brittle fracture [25].

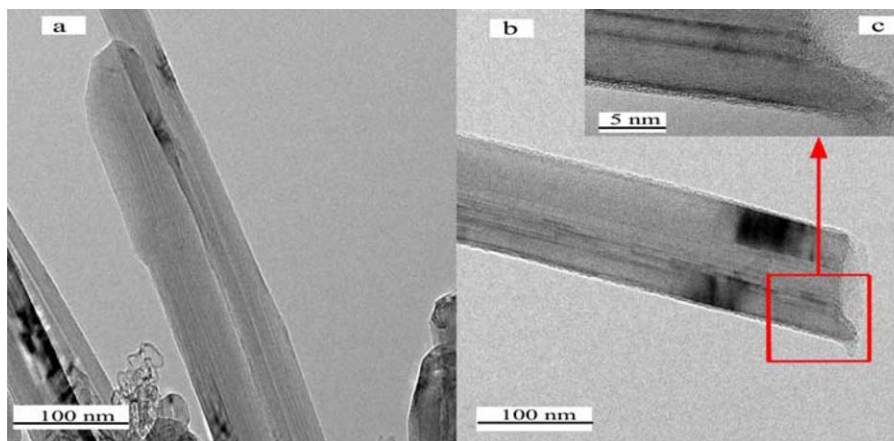


FIG. 5. Surface morphology of VGCNFs (a: raw, b: silanized). [Color figure can be viewed in the online issue, which is available at [wileyonlinelibrary.com](http://wileyonlinelibrary.com).]

### Dynamic Mechanical Analysis

The tangent loss angle of specimens as a function of temperature is shown in Fig. 7. The glass transition temperature of the VGCNF/epoxy composites measured by DMA is given in Table 1. The glass transition temperature ( $T_g$ ) is determined from the peak position of the tangent loss angle. In Fig. 7, in the case of the VGCNF/EP composites with the same content of VGCNFs,  $T_g$  of the raw VGCNF/epoxy is lower than that of the silanized VGCNF/epoxy because the silanized VGCNFs can react with the hardener more completely. This is more pronounced in the case of the silanized VGCNF composite because of the higher degree of cross-linking reactions by the epoxy end-groups of silanized VGCNF than in the case of its raw VGCNF counterpart [25].  $T_g$  decreases with the increase in the loading of the silanized VGCNFs, as shown in Fig. 7. Because the relaxation peak height is associated with molecular mobility, it denotes the highly cross-linked structure at a relatively low silanized-VGCNF content [19]. There is a certain ratio between the epoxy resin and the curing agent. It is suspected that the

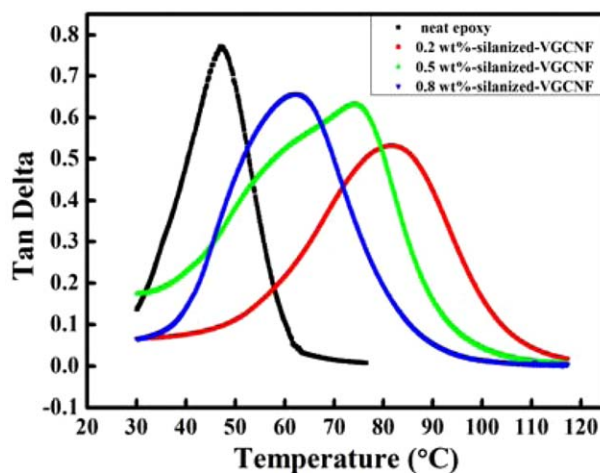


FIG. 7. Tan delta of neat epoxy and silanized-VGCNF/epoxy composites. [Color figure can be viewed in the online issue, which is available at [wileyonlinelibrary.com](http://wileyonlinelibrary.com).]

limited number of silanized sites on VGCNFs can react with the epoxy and the hardener.

### Fold-Deploy Shape Memory Test

Figure 1 shows the test for the shape recovery of specimens. The shape memory property of a representative sample is illustrated in Figs. 8 and 9. The shape recovery ratio curves for VGCNF/EP are presented in

TABLE 1. Glass transition temperature for VGCNF/epoxy composites.

VGCNF content (wt%)	$T_g$ (°C)	
	Raw VGCNF	Silanized VGCNF
0	48	48
0.2	62	82
0.5	66	75
0.8	60	63

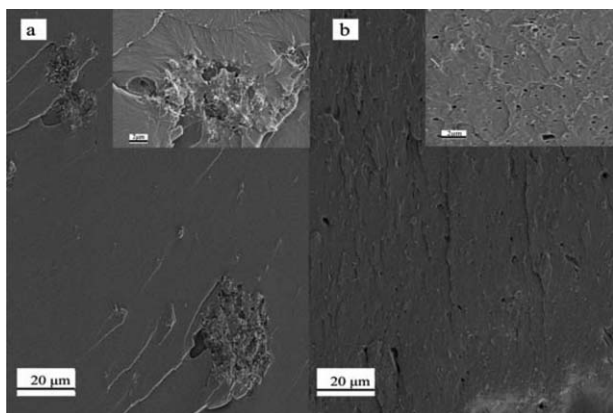


FIG. 6. Cross-section morphology of 0.2 wt% VGCNF/epoxy films (a: raw and b: silanized).

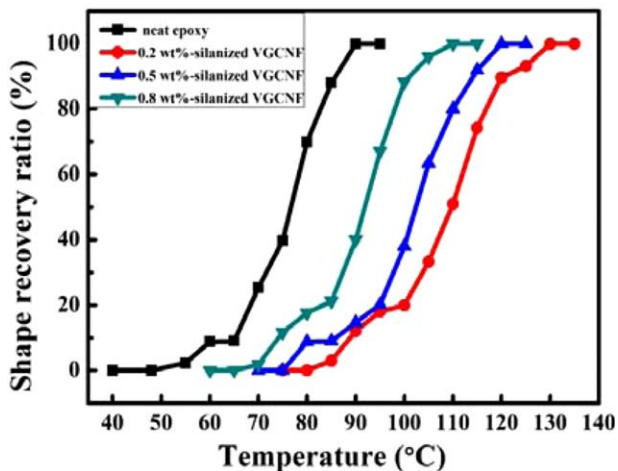


FIG. 8. Shape recovery rates of specimens. [Color figure can be viewed in the online issue, which is available at wileyonlinelibrary.com.]

Fig. 8. All samples have a similar trend that the shape recovery ratio monotonically and sharply increases with an increase in temperature [20]. The figure reveals that the shape memory behavior of silanized VGCNF/EP begins at a higher temperature than that of neat epoxy. Note that 0.2 wt% silanized VGCNF starts exhibiting shape recovery at the highest temperature. This is attributed to the highly cross-linked structures exerting a strong constrained force and the fact that their segments need more energy to move for a higher degree of cross-linking [26].

The shape recovery time for 0.2 wt% silanized VGCNF/EP at different temperatures is shown in Fig. 9. It takes less time to complete the shape recovery process at a relatively high temperature. With an increase in temperature, there is more free volume and more energy for the cross-linked structure. This result agrees with the polymer's time-temperatures superposition principle.

## CONCLUSION

Nanocomposites composed of VGCNFs and epoxy are prepared, and the effects of silanized VGCNFs on the properties of VGCNF/EP nanocomposites are investigated. The major findings from this study are as follows:

1. Silanized VGCNFs are well dispersed in an epoxy matrix, and the interfacial interactions of nanocomposites improve after the silanization treatment.(1).
2. DMA results indicate that the thermo-mechanical properties of VGCNF/EP composites are enhanced by silanized VGCNFs. The glass transition temperature of 0.2 wt% silanized VGCNF/EP nanocomposites increases by 70.8% compared with that of the neat epoxy.(2).
3. The silanized VGCNF/epoxy exhibits excellent shape memory performance. As compared to neat epoxy resins, silanized VGCNF/epoxy can maintain excellent shape recovery even though they have a higher degree of cross-links. The nanocomposites are sensitive to temperature, and it takes less time to complete the shape recovery process at a relatively high temperature.(3).

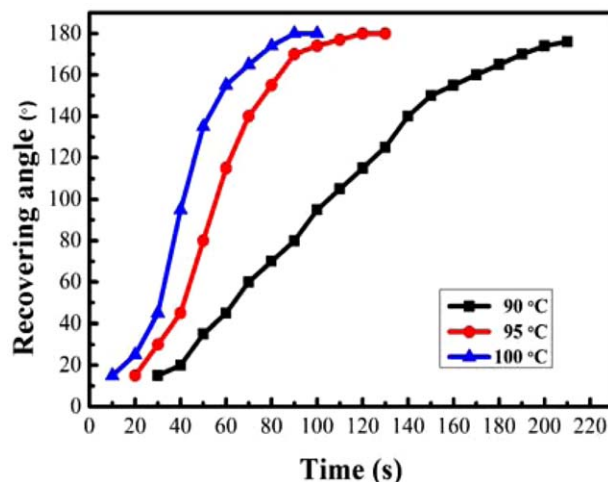


FIG. 9. Shape recovery angle vs. recovering time of 0.2 wt% silanized VGCNF/epoxy resin at different temperatures. [Color figure can be viewed in the online issue, which is available at wileyonlinelibrary.com.]

## ACKNOWLEDGMENT

The authors are grateful for the testing assistance of the instrumental Analysis Center of Zhejiang Sci-Tech University.

## REFERENCES

1. C. Liu, H. Qin, and P.T. Mather, *J. Mater. Chem.*, **7**, 1543 (2007).
2. K. Gall, M.L. Dunn, Y. Liu, and D. Finch, *Acta. Mater.*, **50**, 5115 (2002).
3. D. Ratna and J. K. Kocsis, *J. Mater. Sci.*, **43**, 254 (2008).
4. W.M. Huang, Z. Ding, and C.C. Wang, *Mater. Today*, **13**, 7 (2010).
5. T. Chung, A. Romo Uribe, and P.T. Mather, *Macromolecules*, **41**, 184 (2008).
6. E. Wornyo, K. Gall, F. Yang, and W. King, *Polymer*, **48**, 3213 (2007).
7. T. Xie and I.A. Rousseau, *Polymer*, **50**, 1852 (2009).
8. K.S. Santhosh Kumar and R. Biju, *Polymer*, **73**, 421 (2013).
9. Q.Q. Ni, C.S. Zhang, Y.Q. Fu, G.Z. Dai, and T. Kimrura, *Compos. Struct.*, **81**, 176 (2007).
10. H. Li, J. Zhong, and J. Meng, *Compos. Part B*, **44**, 508 (2013).
11. M.H. Al-Saleh, W.H. Sadaah, and U. Sundararaj, *Carbon*, **47**, 2 (2009).
12. T. Ozkan, M. Naraghi, and I. Chasiotis, *Carbon*, **48**, 239 (2010).
13. M. Endo, Y.A. Kim, T. Hayashi, and K. Nishimura, *Carbon*, **39**, 1287 (2001).
14. G.G. Tibbetts, M.L. Lake, K.L. Strong, and B.P. Rice, *Compos. Sci. Technol.*, **67**, 1709 (2007).
15. K. Zhang and J.Y. Lim, *Diamond Relat. Mater.*, **18**, 316 (2009).
16. P.C. Ma, S.Y. Mo, and B.Z. Tang, *Carbon*, **48**, 1824 (2010).

17. P.C. Ma and A. Naveed, *Compos. Part A*, **41**, 1345 (2010).
18. P.C. Ma, J.K. Kim, and B.Z. Tang, *Carbon*, **44**, 3232 (2006).
19. J.H. Lee, K.Y. Rhee, and S.J. Park, *Compos. Part A*, **42**, 478 (2011).
20. Y.Y. Liu and C.M. Han, *Mater. Sci. Eng. A*, **527**, 2510 (2010).
21. S. Kubota, H. Nishikiori, and N. Tanaka, *J. Phys. Chem. B.*, **109**, 23170 (2005).
22. J. Kathi, K.Y. Rhee, and J.H. Lee, *Compos. Part A*, **40**, 800 (2009).
23. Z. Zhou and S.F. Wang, *Compos. Sci. Technol.*, **68**, 1727 (2008).
24. W. Wood, S. Kumar, and W.H. Zhong, *Macromol. Mater. Eng.*, **295**, 1125 (2010).
25. P.C. Ma, J.K. Kim, and B.Z. Tang, *Compos. Sci. Technol.*, **67**, 2965 (2007).
26. Y.B. Dong, J. Ding, and J. Wang, *Compos. Sci. Technol.*, **76**, 8 (2013).